Quantitative Performance Comparison and Optimization of Novel Complementary Field Excited Linear Flux Switching Machine

Noman ULLAH[1,2], Abdul BASIT[2], Faisal KHAN[1], Faheem ALI[2], Hazrat ALI[1], Rizwan AHMED[1], Imran HASEEB[3], Muhammad Ali KAZMI[1]
[1]*Department of Electrical and Computer Engineering, COMSATS University Islamabad (Abbottabad Campus), Abbottabad, 22060, Pakistan*
[2]*University of Engineering & Technology, Peshawar, 25000, Pakistan*
[3]*Qurtuba University of Science and Information Technology, Dera Ismail Khan, 29050, Pakistan*
nomanullah@cuiatd.edu.pk

***Abstract*—In this paper, two well-known topologies of proposed Double Sided Field Excited Linear Flux Switching Machine with Segmented Secondary (FELFSMSS) i.e. Dual Stator and Dual Mover are quantitatively compared with a valid decision of selecting Dual Stator FELFSMSS (DSFELFSMSS) based on low numerical values of detent force, thrust force ripples, and normal force, and high values of open circuit flux linkage, average thrust force, and thrust force density. In order to uplift overall thrust force profile of selected DSFELFSMSS at the rate of minimum thrust force ripple ratio, geometry based deterministic optimization and appropriate selection of AC and DC current density approach is adopted. Finally, a novel technique of auxiliary end tooth DC winding is applied to limit thrust force ripple ratio less than 10%.**

***Index Terms*—AC machines, brushless motors, electromagnetic devices, design optimization, magnetic flux density.**

I. INTRODUCTION

For more than decades, long stroke applications such as electric trains and skyscrapers' elevator systems are powered by rotary electric motors with mechanical conversion systems. Gearbox is an essential component of conventional installed systems utilized to convert rotating torque into linear thrust force. Mechanical conversion apparatus installed in series with electromechanical system reduces setup's overall efficiency and reliability [1].

Linear electric motor is a revolutionary technology capable of providing direct thrust force, hence eliminating need of mechanical conversion systems [2]. However, linear motors directly obtained by unrolling corresponding rotary designs yields to single sided linear motors [3] and results in high normal (attraction) forces. These undesired y-axis forces exerts additional frictions on bearings and reduces electrical motor's performance [4].

Double sided linear motor topology, accomplished by combining two single sided linear motors can be utilized to curtail high normal force problem with an additional advantage of almost twice average thrust force [5]. Double sided linear motors can be categorized as: (a) Dual stator, and (b) Dual mover. Two movers of single sided linear motor connected back-to-back and constituting a single mover sandwiched between two stators is known as dual stator topology. Whereas, two stator connected in a sequence to develop single stator and encompassed by two separate movers is termed as dual mover topology [6].

Numerous linear motor designs such as linear DC motor, linear synchronous motor, linear switched reluctance motor, and linear induction motor are researched and investigated for various applications. However, all of aforementioned designs limits their applications due to inherent demerits such as low speed-force gradient and high maintenance costs of linear DC motor, increased cost and fixed magnetic flux density of permanent magnets installed on long stator in case of linear synchronous motor, low armature winding utilization ratio and high thrust force ripple ratio associated with linear switched reluctance motor, and requirements of complex control algorithms while handling linear induction motor [7].

Linear Flux Switching Machine (LFSM) is a class of synchronous machine with a modification of confining all excitation sources to short mover. This unique feature enables passive stator (made of only iron) and reduces manufacturing cost due to elimination of stator's permanent magnets when compared with linear PM synchronous machine [8]. LFSM also offers additional advantages of high thrust force/power density, rigid and robust stator, bipolar flux linkage, better temperature control, and suitability for applications where ruggedness and high speed is concerned [9]. LFSMs are researched for various applications such as Maglev transportation and rail transportation [10], subways [11], electromagnetic launch technology [12], linear propulsion technology [13], wave energy generators [14], linear oil pumping actuators [15], artificial hearts [16], long stroke safety-critical applications [17], and low-speed applications [18].

Based on excitation process, LFSM with Segmented Secondary (LFSMSS) can be categorized as; (a) Permanent Magnet LFSMSS (PMLFSMSS), (b) Field Excited LFSMSS (FELFSMSS), and (c) Hybrid Excited LFSMSS (HELFSMSS). AC windings and PMs are used for excitation purposes of PMLFSMSS. Similarly, AC windings and field (DC) windings are excited for FELFSMSS. Whereas, AC windings, PMs, and field (DC) windings are combined to excite HELFSMSS [7]. Numerous models of

Digital Object Identifier 10.4316/AECE.2019.04002

PMLFSMSS are researched for different applications due to capability of producing high thrust force density. However, cost of rare earth PM material has been increased in past few years and secondly PMs are only able to generate fixed air-gap magnetic flux densities [19]. Aforementioned problems associated with PMLFSMSS can be curtailed by adopting FELFSMSS or HELFSMSS. HELFSMSS has relatively complex magnetic structure and flux weakening process may demagnetize PMs installed within same mover [9].

FELFSMSS are preferred for long stroke applications due to their unique advantages of: (a) elimination of mechanical conversion system when compared with corresponding rotary designs, (b) low cost and variable air-gap magnetic flux density when compared with PMLFSMs, and (c) segmented secondary reduces volume and cost of long stator when compared with uniform secondary. Additionally, complementary design of proposed machine results in more symmetric flux linkage waveforms. In this paper, two double sided FELFSMs having same design dimensions, magnetic loadings, and electric loadings are proposed and quantitatively compared in Section II. Detailed analysis and comparison revealed that dual stator FELFSMSS shows better performance in terms of peak-to-peak flux linkage, peak-to-peak detent force, average thrust force, peak-to-peak normal force, and thrust force ripple ratio. Upon successful selection, dual stator FELFSMSS is subjected to geometry based deterministic optimization (GDO) approach followed by search for appropriate AC and DC current densities to achieve minimum thrust force ripple ratio and uplift overall thrust force profile, in Section III. In order to limit thrust force ripple ratio within 10% range, a novel technique of auxiliary end tooth DC winding is proposed and simulated in Section IV. Finally, some conclusions are drawn in Section V.

II. DESIGN TOPOLOGIES AND COMPARISONS

A. Topologies and Design Methodology

While considering applications' requirements, proposed double sided FELFSMSS having two unique inherent properties i.e. field coils to replace PMs and segmented secondary in place of long uniform secondary helps to reduce overall manufacturing cost with additional benefits of LFSMs defined earlier in Section 1. However, these unique features can be enabled by two different designs i.e. Dual Stator FELFSMSS (DSFELFSMSS) and Dual Mover FELFSM (DMFELFSMSS) topology.

Both of aforementioned topologies (shown in Fig. 1) are simulated using Finite Element Method (FEM) utilizing JMAG Commercial FEA Package v. 14.1. Design of proposed FELFSMSSs is complementary in nature and following equations are utilized to determine number of mover teeth (N_{mt}), number of DC coil pairs (N_{DC}), number of AC coil pairs (N_{AC}), and stator to mover pole pitch (τ_s/τ_m) [20]:

$$N_{mt} = 4jm + 1 \tag{1}$$

$$N_{DC} = 2jm + 1 \tag{2}$$

$$N_{AC} = 2jm \tag{3}$$

$$\tau_s / \tau_m = 4jm / (2jm + 2) \tag{4}$$

Where m represents number of phases, j is a positive integer and represents each AC phase winding pair repetition in the machine, τ_s is the stator pole pitch, and τ_m is mover pole pitch. Double sided FELFSMSSs having dual stator and dual mover topologies with single side specifications of m=3; j=2; N_{mt}=25; N_{DC}=13; and N_{AC}=12 leading to τ_s/τ_m= 24/14 are investigated in this paper. Additional teeth on all four corners are attached to balance magnetic circuit.

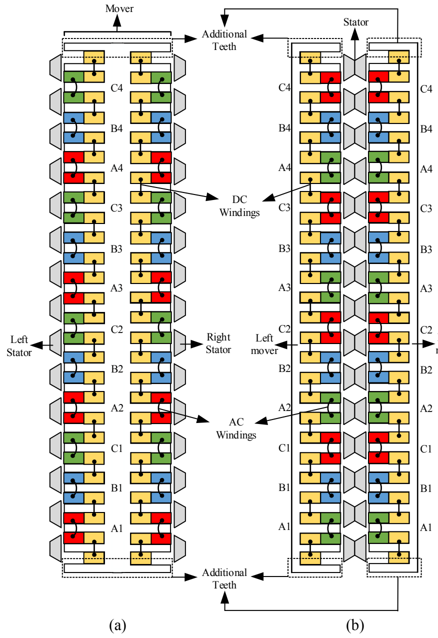

Figure 1. 2D cross section of double sided FELFSMSS; (a) Dual stator FELFSMSS, and (b) Dual mover FELFSMSS

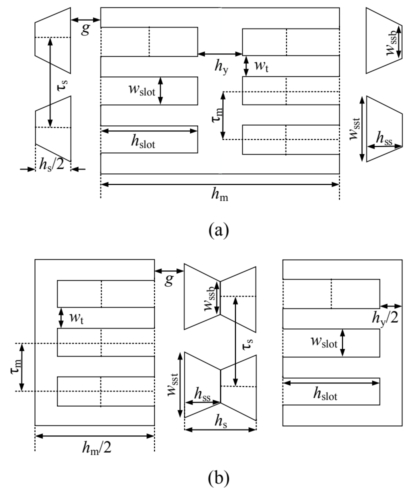

Figure 2. Design variables of double sided FELFSMSS; (a) Dual stator FELFSMSS, and (b) Dual mover FELFSMSS

Design variables and parameters for both topologies are kept constant and are shown in Fig. 2 and Table I, respectively.

B. Comparison of DSFELFSMSS and DMFELFSMSS

Five important key performance indicators termed as peak-to-peak open circuit flux linkage of center phase (*Flux-Linkage*$_{p-p}$), peak-to-peak detent force (*Detent-Force*$_{p-p}$), average thrust force (*Thrust-Force*$_{Avg}$), peak-to-peak normal force (*Normal-Force*$_{p-p}$), thrust force ripple ratio (*TFRR*), and their corresponding waveforms are considered for detailed comparison of both topologies. All key performance indicators except *TFRR* can be directly obtained by FEM, Equation (5) is utilized to calculate *TFRR* [8];

$$TFRR = \frac{Thrust - Force_{Rip}}{Thrust - Force_{Avg}} * 100\% \quad (5)$$

Where;

$$Thrust - Force_{Rip} = TForce_{Max} - TForce_{Min} \quad (6)$$

Here, $Thrust\text{-}Force_{Rip}$, $TForce_{Max}$, $TForce_{Min}$ represents thrust force ripples, maximum thrust force, and minimum thrust force, respectively.

TABLE I. DESIGN PARAMETERS OF DOUBLE SIDED FELFSMSS

Parameter, Symbol, Unit	Value	
	Dual Stator FELFSMSS	Dual Mover FELFSMSS
Mover pole pitch, τ_m, mm	17.5	
Stator pole pitch, τ_s, mm	30	
Mover height, h_m, mm	85	
Stator height, h_s, mm	25	
Mover tooth width, w_t, mm	7.5	
Slot width, w_{slot}, mm	10	
Slot height, h_{slot}, mm	35	
Mover yoke height, h_y, mm	15	
Air-gap, g, mm	0.5	
Stator segment tip width, w_{sst}, mm	24	
Stator segment base width, w_{ssb}, mm	12	
Stator segment height, h_{ss}, mm	12.5	
Stack length, L, mm	100	
Slot area, A_{slot}, mm^2	350	
Mover velocity, v, m/s	0.5	
Number of AC coil turns, N_{AC}	40	
Number of DC coil turns, N_{DC}	40	
AC and DC winding fill factor, k_f	0.5	
AC current density, J_{AC}, A/mm^2	0.55	
DC current density, J_{DC}, A/mm^2	0.80	
Whole machine height, h_{wm}, mm	111	
Split ratio, $S.R$	0.2342	

Three phase open circuit flux linkage of both topologies is compared in Fig. 3. It can be seen that, both topologies waveforms follows same pattern with a dissimilarity that DSFELFSMSS shows high flux linkage in magnitude. Reason behind high flux linkage is physical structure of dual stator topology that reduces flux leakage, as flux generation and linkage mover volume is surrounded by two stators. It should also be noticed that open circuit flux linkage of dual stator topology is more symmetric in terms of y-axis magnitude at both positive and negative peaks. Detent force waveforms obtained from FEM are also compared and shown in Fig. 4. Almost same waveform pattern is observed for both topologies. However, DSFELFSMSS waveform show reduced peaks on both y-axis extremes ($Detent\text{-}Force_{p\text{-}p}$ = 6.24N), when compared with dual mover topology. These reduced peaks results in reduced $Detent\text{-}Force_{p\text{-}p}$, vibrations, and corresponding acoustic noise.

Detent force is a no-load parameter (when only DC excitation is applied) and results in thrust force ripples when on-load condition (when both AC and DC excitations are applied) is investigated [21]. Thrust force ripples is an undesired parameter and helps to calculate *TFRR*. Aforementioned statement is verified by observing thrust force waveform shown in Fig. 5. Detailed analysis revealed that, range of electrical angle where detent force value is positive produced a push in thrust force waveform at the same electrical angles. Similarly, negative values of detent force resulted as pull in the thrust force waveform. This undesired push and pull gave birth to maximum and minimum thrust force values, difference of maximum and minimum values results in thrust force ripples, and eventually thrust force ripple ratio. While comparing thrust force waveform, DSFELFSMSS topology shows high numerical values that resulted in high $Thrust\text{-}Force_{Avg}$. *TFRR* for both topologies is also calculated and is illustrated in Table II.

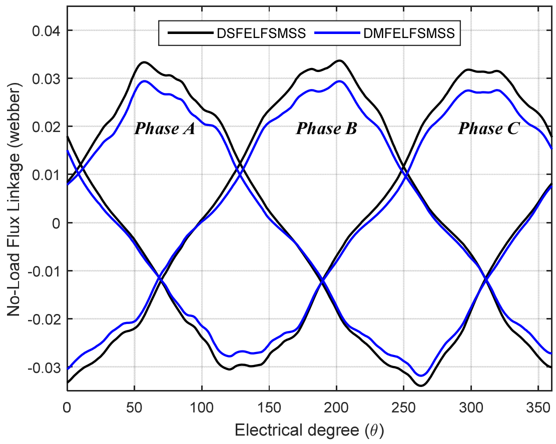

Figure 3. Three phase no-load flux linkage comparison

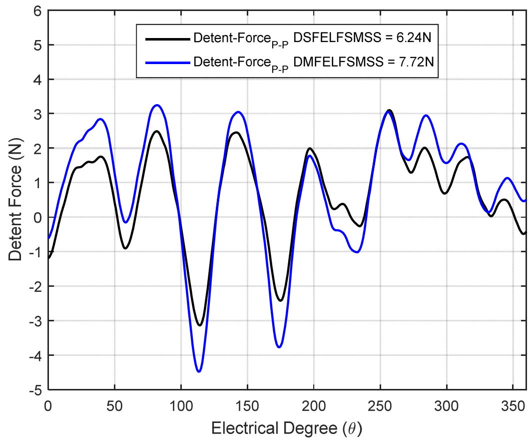

Figure 4. Detent force comparison

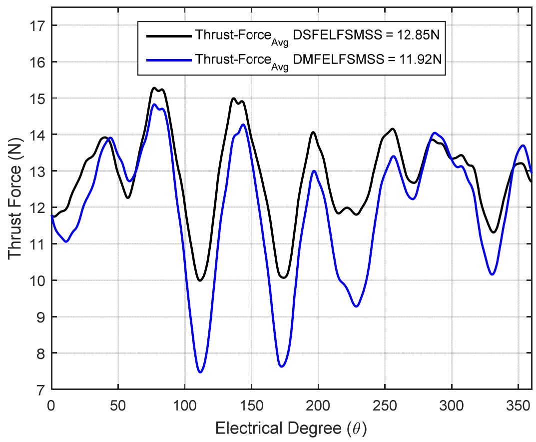

Figure 5. Thrust force comparison

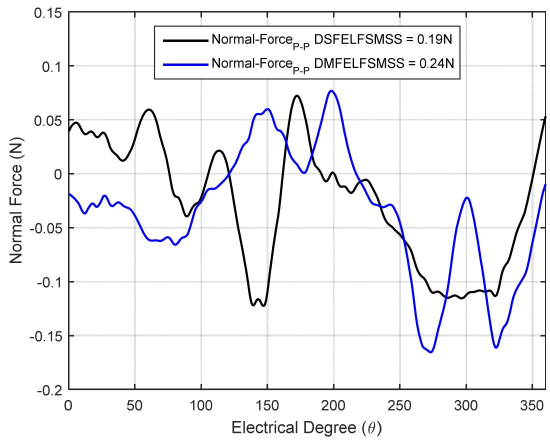

Figure 6. Normal force comparison

TABLE II. QUANTITATIVE COMPARISON OF DSFELFSMSS AND DMFELFSMSS

Key Performance Indicator (Unit)	Value	
	DSFELFSMSS	**DMFELFSMSS**
Flux-Linkage$_{p-p}$ (mWb)	67.20	61.26
Detent-Force$_{p-p}$ (N)	6.24	7.72
Thrust-Force$_{Avg}$ (N)	12.85	11.92
Normal-Force$_{p-p}$ (N)	0.19	0.24
TFRR (%)	41.22	61.72

Normal force waveforms for both topologies are compared and are presented in Fig. 6. Although both topologies shows bipolar normal force with average value of almost zero Newton, DSFELFSMSS wins the race with additional advantage of lower peak-to-peak value. Quantitative comparison of both topologies is tabulated in Table II.

Based on aforementioned analyses and comparisons, DSFELFSMSS is concluded as a better model compared to DMFELFSMSS, and is selected for further analysis.

III. OPTIMIZATION APPROACH AND APPROPRIATE CURRENT DENSITIES SELECTION

A. Geometry based Deterministic Optimization

DSFELFSMSS is subjected to geometry based deterministic optimization (GDO) approach in order to investigate optimal split ratio, stator height, mover height, AC and DC winding slot width and slot height, mover tooth width, mover yoke height, stator segment tip width, and stator segment base width. All other parameters such as mover pole pitch, stator pole pitch, air-gap, stack length, slot area, mover velocity, number of AC and DC winding turns, and whole machine height are kept constant. Also AC and DC current densities are kept constant during whole geometric optimization approach.

GDO leads to a sequential local optimal solutions of geometry parameters and is advantageous in reduction of computational complexity and time consumption, when compared with advanced simultaneous optimization techniques. It is important to mention that due to sequential nature, every consequent optimization variable may or may not depend upon a previous variable value. GDO ensures investigation of leading geometry parameters that influence machine's performance [22].

Increase of average thrust force is set as a priority for the selection of machine configuration. In order to distinguish base and optimized machine configurations illustrated in subsequent figures, methodology of encircling with different colors is used. The base machine configuration is indicated in black, whereas the optimized machine configuration is shown in green.

In order to optimize nine geometry parameters (mentioned before), following four optimization coefficients are defined.

$$S.R = \frac{(h_s + 2g)}{(h_s + 2g + h_m)} \tag{7}$$

$$K_{slot\,\dim} = \frac{w_{slot}}{h_{slot}} \tag{8}$$

$$K_{sstw} = \frac{w_{sst}}{\tau_s} \tag{9}$$

$$K_{ssbw} = \frac{w_{ssb}}{w_{sst}} \tag{10}$$

Where, $K_{slotdim}$ is AC and DC winding slot area dimension coefficient, K_{sstw} and K_{ssbw} are stator segment tip and base width coefficient, respectively. Initial values of optimization geometry parameters, optimization order and coefficients, and corresponding constraints are listed in Table I and Table III, respectively.

TABLE III. OPTIMIZATION SEQUENCE, COEFFICIENTS, AND CONSTRAINTS

Sequence	Coefficient	Initial Value	Constraints
1	*S.R*	0.2342	[0.2000-0.3603]
2	$K_{slotdim}$	0.2857	[0.1828-0.4113]
3	K_{sstw}	0.800	[0.650-0.900]
4	K_{ssbw}	0.457	[0.076-1.000]

1) Split Ratio Optimization

Split ratio can be defined as ratio of stator to whole machine volume. As in case of DSFELFSMSS, stack length for stator and mover is same, hence only height is considered in optimization coefficient presented in Equation (7). Initial value tabulated in Table III can be calculated from data provided in Table I. Whereas, constraints of optimization coefficients are restricted according to general machine design rules and are justified according to geometry. As proposed machine represents segmented secondary, each segment laminations are to be packed with help of supporting bolt system, hence minimum height of each segment is limited to 10.5mm and yields to minimum *S.R=0.20*. Further reduction in *S.R* may not be possible due to manufacturing constraints. Maximum value of *S.R* is limited by mover yoke height as winding slot area dimensions are kept constant. Increase in *S.R* represent decrease in mover volume and ultimately mover yoke height. *S.R* is increased up to limit that mover yoke height of 1mm (equals to *S.R*=0.3603) is achieved. Further increment is not possible due to manufacturing constraints.

DSFELFSMSS with different *S.Rs* are simulated, investigated, and three important key performance indicators i.e. *Thrust-Force$_{Avg}$*, *Detent-Force$_{p-p}$*, and *TFRR* are compared in Fig. 7. It can be seen that, *Thrust-Force$_{Avg}$* plot shows decreasing nature whereas *Detent-Force$_{p-p}$*, and *TFRR* shows increasing behavior with increase in *S.R*. While analyzing manufacturing cost, DSFELFSMSS with reduced *S.R* is preferred because the proposed machine is to be installed as long stroke application design and reduced

S.R means reduced long stator volume. Based on above analysis and considering maximum *Thrust-Force*$_{Avg}$, DSFELFSMSS with *S.R*=0.20 is selected as optimal machine configuration and is termed as DSFELFSMSS-Optimized 1 (DSFELFSMSS-Op1) in this paper. Detailed comparison of DSFELFSMSS and DSFELFSMSS-Op1 is illustrated in Table IV.

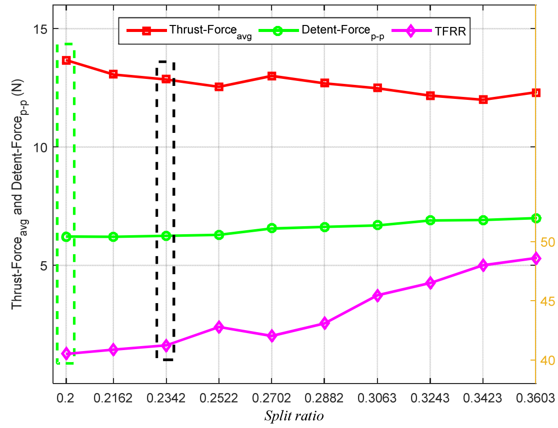

Figure 7. Influence of *S.R* on performance of DSFELFSMSS

TABLE IV. QUANTITATIVE COMPARISON OF DSFELFSMSS AND DSFELFSMSS-OP1

Key Performance Indicator (Unit)	Value	
	DSFELFSMSS	DSFELFSMSS-Op1
Flux-Linkage$_{p-p}$ (mWb)	67.20	69.94
Detent-Force$_{p-p}$ (N)	6.24	6.21
Thrust-Force$_{Avg}$ (N)	12.85	13.67
Normal-Force$_{p-p}$ (N)	0.19	0.19
TFRR (%)	41.22	40.50

2) Winding Slot Area Dimensions Optimization

Width and height of AC and DC winding slot are important factors controlling winding slot opening, mover tooth width, and mover yoke height, and are optimized while keeping winding slot area constant. Maximum and minimum limit of optimization coefficient (Equation (8)) defined in Table III are restricted by mover tooth width and mover yoke height. Winding slot width and height are altered subject to condition that overall slot area remains constant. Initially, winding slot height is increased and slot width is decreased up to limit that mover yoke height of 1.5mm is achieved and this practice resulted in minimum limit of constraints defined in Table III. Any further reduction in Equation (8) may cause critical magnetic saturation at mover yoke height.

As defined optimization coefficient is directly proportional to winding slot width, while keeping mover pole pitch constant, mover tooth width must be reduced to increase slot width. Minimum value of mover tooth width considered in this study is 5.5mm and yields to maximum value of optimization coefficient defined in Table III. Further theoretical increase in limits of Equation (8) resulted in a very narrow mover tooth width and may result in magnetic saturation. Results for three important key performance indicators while analyzing DSFELFSMSS-Op1 having different $K_{slotdim}$ is presented in Fig. 8. It can be observed that, maximum *Thrust-Force*$_{Avg}$ can be achieved by selecting w_t=9.5mm, w_{slot}=8mm, h_{slot}=43.75mm, and h_y=1.5mm. Hence, DSFELFSMSS-Op1 with $K_{slotdim}$=0.1828 is selected as optimal machine configuration and is termed as DSFELFSMSS-Optimized 2 (DSFELFSMSS-Op2) in this paper. Detailed comparison of DSFELFSMSS-Op1 and DSFELFSMSS-Op2 is illustrated in Table V.

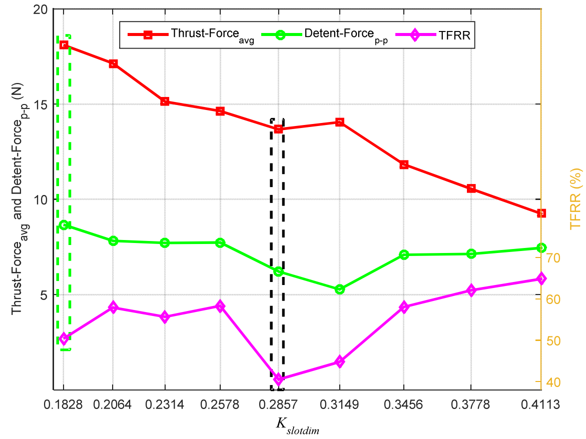

Figure 8. Influence of $K_{slotdim}$ on performance of DSFELFSMSS-Op1

TABLE V. QUANTITATIVE COMPARISON OF DSFELFSMSS-OP1 AND DSFELFSMSS-OP2

Key Performance Indicator (Unit)	Value	
	DSFELFSMSS-Op1	DSFELFSMSS-Op2
Flux-Linkage$_{p-p}$ (mWb)	69.94	78.91
Detent-Force$_{p-p}$ (N)	6.21	8.67
Thrust-Force$_{Avg}$ (N)	13.67	18.10
Normal-Force$_{p-p}$ (N)	0.19	5.24
TFRR (%)	40.50	50.38

3) Stator Segment Tip Width Optimization

Each stator segment optimization is important due to the fact that proposed machine is designed for long stroke application having almost infinite length of stator. Due to segmented secondary nature, each stator module is sole path to complete magnetic structure and stator segment area facing mover (termed as stator segment tip width) is a crucial parameter to complete the magnetic structure. Stator pole pitch is kept constant whereas stator segment tip width is varied with the help of optimization coefficient defined in Equation (9).

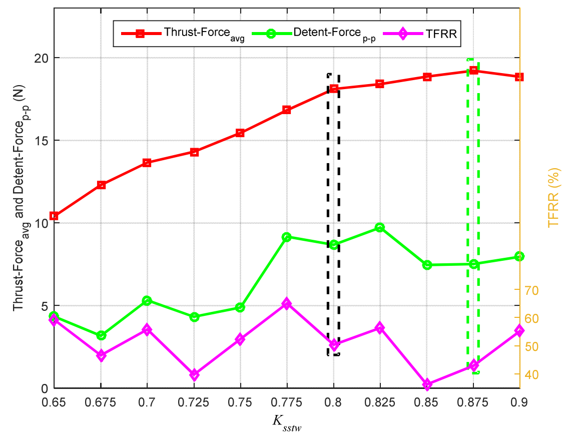

Figure 9. Influence of K_{sstw} on performance of DSFELFSMSS-Op2

Maximum limit of optimization coefficient is when stator segment covers 90% of stator pole pitch due to fact that in case of further increment, proposed machine may loss its segmented secondary nature. Minimum value of Equation (9) can be further reduced from the value depicted in Table III. However, further reduction demolish *Thrust-Force*$_{Avg}$ performance and is set as 0.65. DSFELFSMSS-Op2 having different stator segment tip widths are compared and depicted in Fig. 9. It can be seen that, *Thrust-Force*$_{Avg}$ plot goes on increasing up to value of w_{sst}=26.25mm and then goes on decreasing. Hence, DSFELFSMSS-Op2 with K_{sstw}=0.875 is selected as optimal machine configuration and is termed as DSFELFSMSS-Optimized 3 (DSFELFSMSS-Op3) in this paper. Detailed comparison of DSFELFSMSS-Op2 and DSFELFSMSS-Op3 is illustrated in Table VI.

TABLE VI. QUANTITATIVE COMPARISON OF DSFELFSMSS-OP2 AND DSFELFSMSS-OP3

Key Performance Indicator (Unit)	Value	
	DSFELFSMSS-Op2	DSFELFSMSS-Op3
Flux-Linkage$_{p\text{-}p}$ (mWb)	78.91	89.09
Detent-Force$_{p\text{-}p}$ (N)	8.67	7.50
Thrust-Force$_{Avg}$ (N)	18.10	19.21
Normal-Force$_{p\text{-}p}$ (N)	5.24	0.02
TFRR (%)	50.38	42.89

4) Stator Segment Base Width Optimization

With respect to updated stator segment tip width (w_{sst}=26.25mm), stator segment base width should also be investigated to achieve an optimized stator for proposed machine. Considering manufacturing constraints, minimum value of stator segment base width is considered as 2mm yielding to optimization coefficient defined in Equation (10) of 0.076. Whereas, maximum value is when stator segment base width is equal to stator segment tip width.

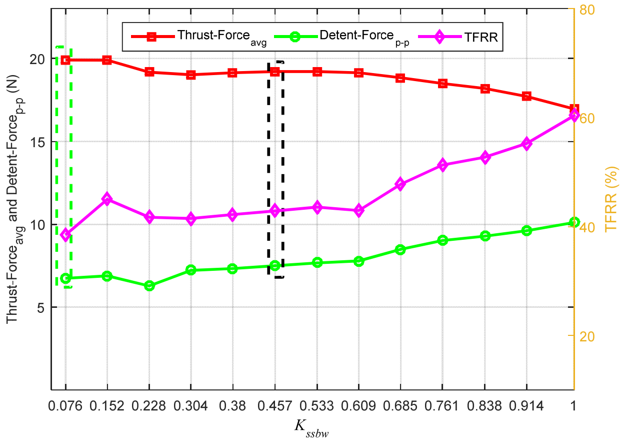

Figure 10. Influence of K_{ssbw} on performance of DSFELFSMSS-Op3

TABLE VII. QUANTITATIVE COMPARISON OF DSFELFSMSS-OP3 AND DSFELFSMSS-OP4

Key Performance Indicator (Unit)	Value	
	DSFELFSMSS-Op3	DSFELFSMSS-Op4
Flux-Linkage$_{p\text{-}p}$ (mWb)	89.09	96.08
Detent-Force$_{p\text{-}p}$ (N)	7.50	6.74
Thrust-Force$_{Avg}$ (N)	19.21	19.91
Normal-Force$_{p\text{-}p}$ (N)	0.02	0.02
TFRR (%)	42.89	38.47

Again, important key performance indicators of DSFELFSMSS-Op3 having different K_{ssbw} is presented in Fig. 10. It can be observed that, maximum *Thrust-Force*$_{Avg}$ and minimum *TFRR* can be achieved by selecting w_{ssb}=2mm. Furthermore, from machining point of view, reduced value of stator base optimization coefficient will result in reduced manufacturing cost and stator segment volume. Hence, DSFELFSMSS-Op3 with K_{ssbw}=0.076 is selected as optimal machine configuration and is termed as DSFELFSMSS-Optimized 4 (DSFELFSMSS-Op4) in this paper. Detailed comparison of DSFELFSMSS-Op3 and DSFELFSMSS-Op4 is illustrated in Table VII. Geometric parameters modified/optimized during GDO approach are tabulated in Table VIII.

TABLE VIII. UPDATED DESIGN PARAMETERS DURING GDO APPROACH

Parameter, Unit	Value	
	DSFELFSMSS	DSFELFSMSS-Op4
h_m, mm	85	89
h_s, mm	25	21
w_t, mm	7.5	9.5
w_{slot}, mm	10	8
h_{slot}, mm	35	43.75
h_y, mm	15	1.5
w_{sst}, mm	24	26.25
w_{ssb}, mm	12	2
h_{ss}, mm	12.5	10.5
S.R	0.2342	0.20

B. AC and DC Current Densities Selection

In order to achieve minimum *TFRR* with appropriate *Thrust-Force*$_{Avg}$ and examine overload capability of DSFELFSMSS-Op4 without any special cooling arrangements, search for appropriate AC and DC current densities (J_{AC} and J_{DC}) is done in this section. According to literature, an electrical machine can be excited up to maximum current density of 30A/mm^2 without any special cooling arrangements [23]. Hence, observing aforementioned constraint both J_{AC} and J_{DC} are increased in small interval steps and performance of DSFELFSMSS-Op4 is evaluated in terms of *Thrust-Force*$_{Avg}$ and *TFRR*, as shown in Fig. 11.

It can be observed that, *Thrust-Force*$_{Avg}$ plot increases almost linearly with increase of J_{AC} and J_{DC} throughout the range, hence validating overload thrust force capability. However, *TFRR* plot decreases up to a specific range and then goes on increasing. As purpose of these current densities' search is defined earlier, DSFELFSMSS-Op4 having *Thrust-Force*$_{Avg}$ = 1347.30N and minimum *TFRR* (12.74%) is achieved by applying J_{AC} = 10.74 A/mm^2 and J_{DC} = 15.35 A/mm^2 is selected and subjected to further analysis. Detailed comparison of DSFELFSMSS-Op4 performance having initially designed and updated J_{AC} and J_{DC} is done in Table IX.

TABLE IX. COMPARISON OF DSFELFSMSS-OP4 PERFORMANCE WITH INITIALLY DESIGNED AND UPDATED CURRENT DENSITIES

Key Performance Indicator (Unit)	DSFELFSMSS-Op4 Performance	
	J_{AC}=0.55, J_{DC}=0.80 (A/mm^2)	J_{AC}=10.74, J_{DC}=15.35 (A/mm^2)
Flux-Linkage$_{p\text{-}p}$ (mWb)	96.08	439.41
Detent-Force$_{p\text{-}p}$ (N)	6.74	155.42
Thrust-Force$_{Avg}$ (N)	19.91	1347.30
Normal-Force$_{p\text{-}p}$ (N)	0.02	5.28
TFRR (%)	38.47	12.74

IV. AUXILIARY END TOOTH DC WINDING TECHNIQUE

In order to limit *TFRR* below 10%, a novel *TFRR* reduction methodology termed as auxiliary end tooth DC winding technique is proposed. According to the strategy, all four end teeth are wound with a coil having number of turns equal to armature winding. When DC current is supplied to the end winding, it reshapes the end tooth magnetic circuit and modifies thrust force ripples caused by end effect [24]. Geometric modification done in DSFELFSMSS-Op4 is shown in Fig. 12.

The technique is implemented as two step remedy. Initially, all sixteen dot cross combinations of auxiliary end tooth DC winding having current density (J_{ETDC} = 15.35 A/mm^2) equal to other DC windings. As can be seen in Fig. 13, minimum *TFRR* of 12.23% can be achieved with a minimal decrement in *Thrust-Force$_{Avg}$*. Hence, DSFELFSMSS-Op4 with end tooth DC winding having J_{ETDC} = 15.35 A/mm^2 is selected for further analysis. Detailed comparison of DSFELFSMSS-Op4 with and without auxiliary end tooth DC winding is illustrated in Table X.

However, the first step was unable to meet the requirements (*TFRR* below 10%). Hence, in the second step J_{ETDC} is varied from 0 A/mm^2 to 30 A/mm^2 and results for *Thrust-Force$_{Avg}$* and *TFRR* are presented in Fig. 14. It can be observed that, auxiliary end tooth DC winding current density constructively modifies magnetic structure of proposed machine up to a specific range and then shows adverse effect. It can also be noticed that, minimum *TFRR* of 9.46% is obtained by selecting J_{ETDC} = 7.27 A/mm^2. Detailed comparison of DSFELFSMSS-Op4 with J_{ETDC} = 15.35 A/mm^2 and 7.27 A/mm^2 is done in Table XI.

TABLE X. COMPARISON OF DSFELFSMSS-OP4 PERFORMANCE WITH AND WITHOUT AUXILIARY END TOOTH DC WINDING

Key Performance Indicator (Unit)	DSFELFSMSS-Op4 Performance	
	Without auxiliary end tooth DC winding	Auxiliary end tooth DC winding with J_{ETDC}=15.35 (A/mm^2)
Flux-Linkage$_{p-p}$ (mWb)	439.41	439.02
Detent-Force$_{p-p}$ (N)	155.42	175.53
Thrust-Force$_{Avg}$ (N)	1347.30	1344.73
Normal-Force$_{p-p}$ (N)	5.28	6.21
TFRR (%)	12.74	12.23

TABLE XI. COMPARISON OF DSFELFSMSS-OP4 PERFORMANCE WITH DIFFERENT J_{ETDC}

Key Performance Indicator (Unit)	DSFELFSMSS-Op4 Performance	
	Auxiliary end tooth DC winding with J_{ETDC}=15.35 (A/mm^2)	Auxiliary end tooth DC winding with J_{ETDC}=7.27 (A/mm^2)
Flux-Linkage$_{p-p}$ (mWb)	439.02	439.25
Detent-Force$_{p-p}$ (N)	175.53	184.57
Thrust-Force$_{Avg}$ (N)	1344.73	1359.99
Normal-Force$_{p-p}$ (N)	6.21	7.41
TFRR (%)	12.23	9.46

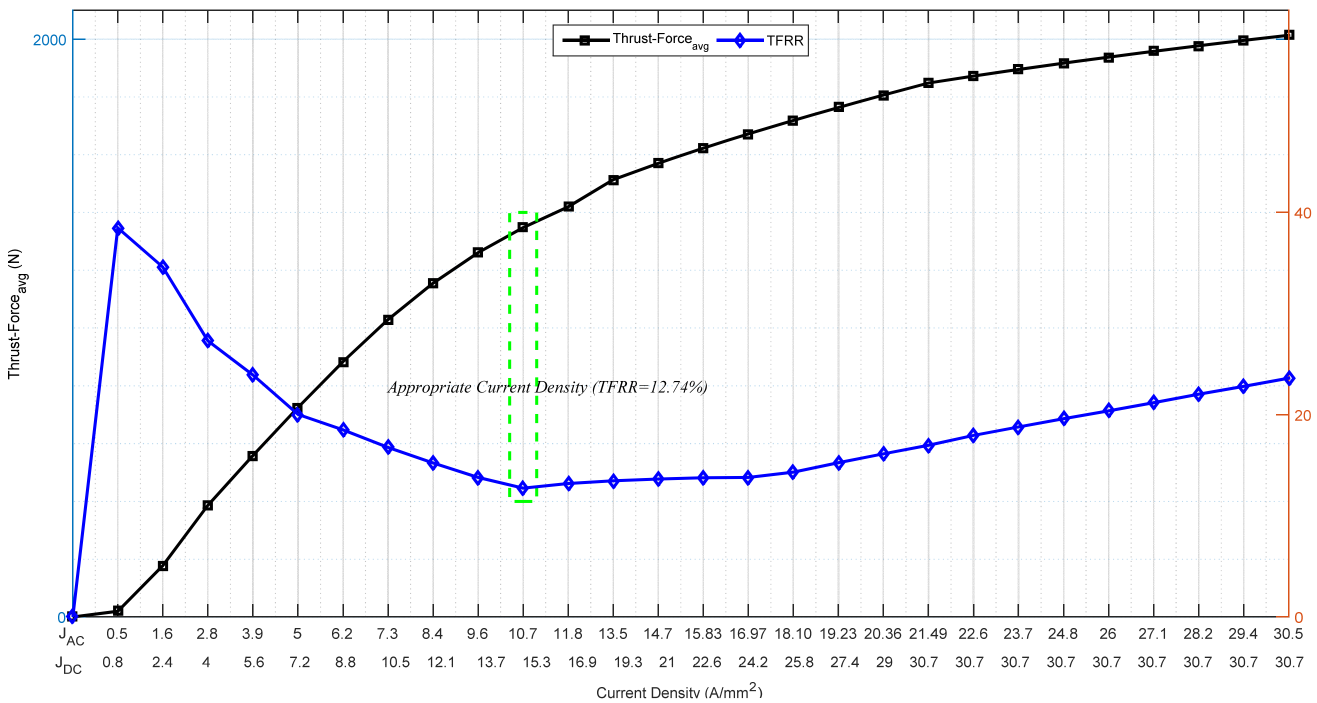

Figure 11. Performance of DSFELFSMSS-Op4 with different J_{AC} and J_{DC}

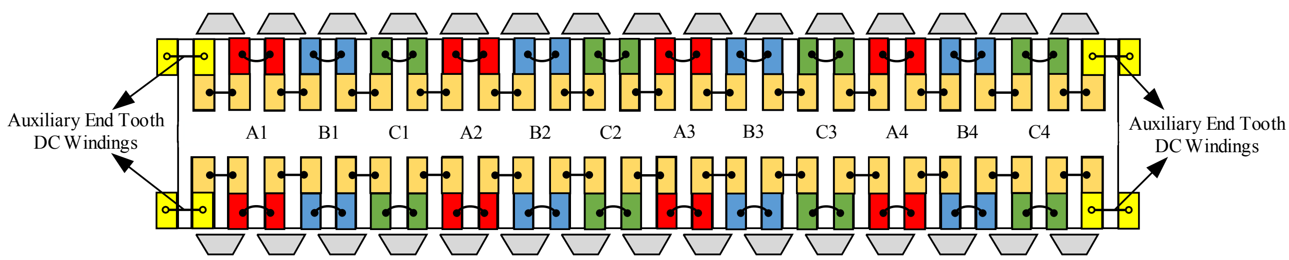

Figure 12. Geometric modification due to Auxiliary End Tooth DC Winding

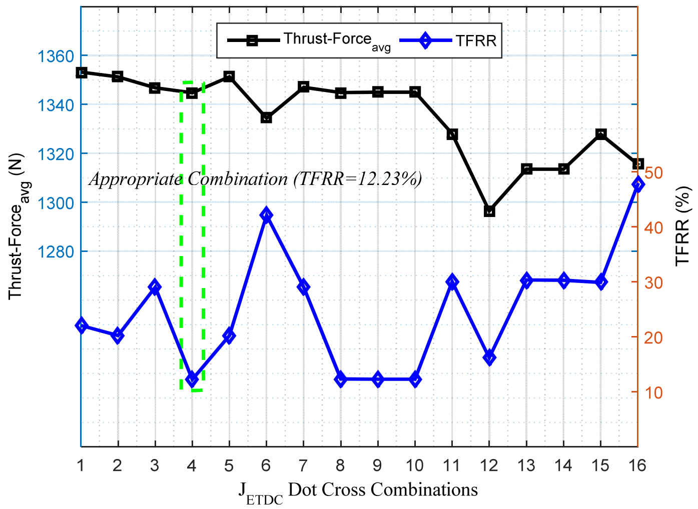

Figure 13. Performance of modified DSFELFSMSS-Op4 having different Auxiliary End Tooth DC winding dot cross combinations

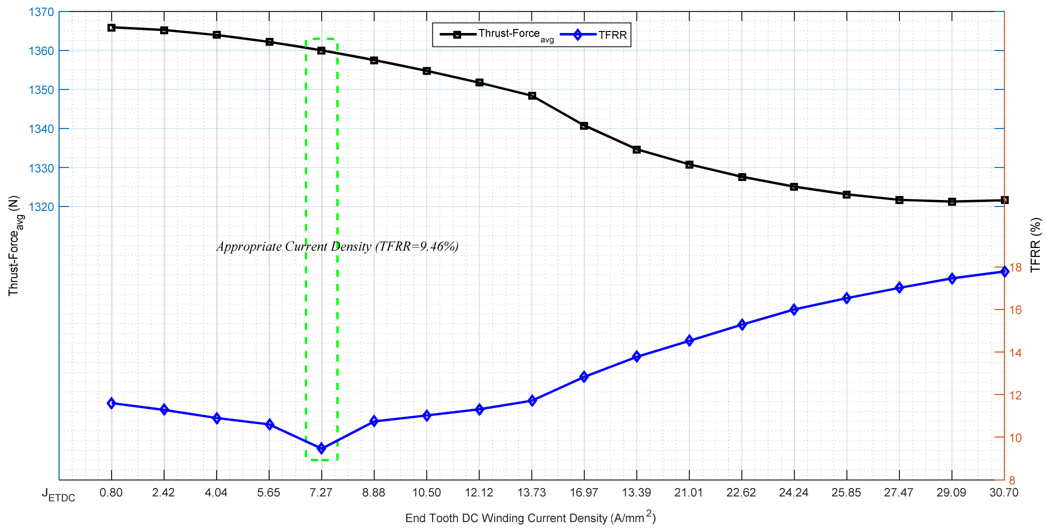

Figure 14. Performance of modified DSFELFSMSS-Op4 with different J_{ETDC} values

As the desired objectives are accomplished, detailed comparison of all five key performance indicators' waveforms and numerical values is done for DSFELFSMSS and modified DSFELFSMSS-Op4 in Fig. 15-18 and Table XII. Comparison is intended to validate the performance of optimization approach and novel *TFRR* reduction technique.

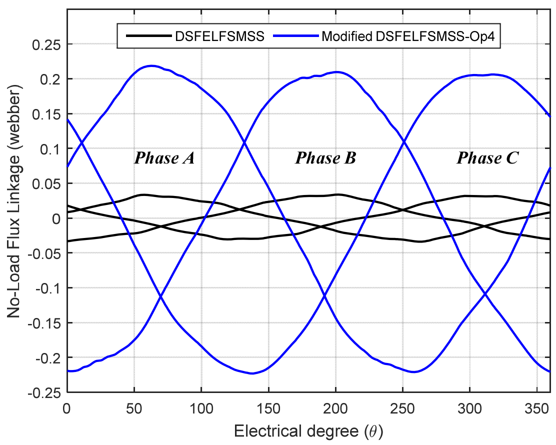

Figure 15. Three phase no-load flux linkage comparison

It can be seen that, modified DSFELFSMSS-Op4 no-load three phase flux linkage is higher in magnitude, symmetrical along y-axis, and more sinusoidal compared to initial model (as shown in Fig. 15). While analyzing detent force waveforms (Fig. 16), *Detent-Force*$_{p-p}$ of modified and optimized model is higher than initial model, it is understood that whenever an increase or uplift in thrust force waveform is achieved, detent force value will also increase. Thrust force waveform comparison presented in Fig. 17 indicates that *Thrust-Force*$_{Avg}$ of optimized and modified model is 105 times more than that of initial model. Ratio of increase in *Thrust-Force*$_{Avg}$ is more than *Detent-Force*$_{p-p}$.

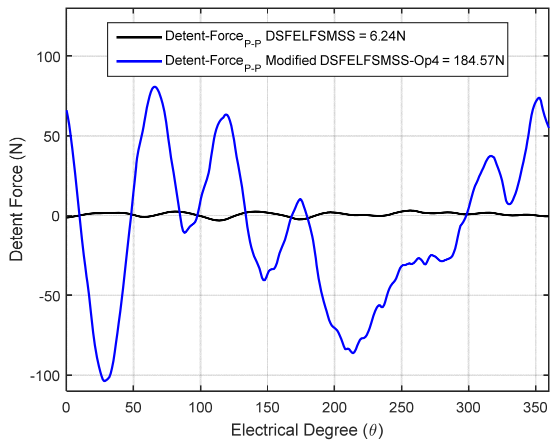

Figure 16. Detent force comparison

Hence suppressing 30 times increment of *Detent-Force*$_{p-p}$.

TFRR is also reduced from 41.22% to 9.46%. Finally, normal force waveforms are compared in Fig. 18. Although *Normal-Force$_{p\text{-}p}$* associated with optimized and modified model is more than that of initial model. However, normal force waveform is bipolar and its average value for each electrical cycle is almost zero [25].

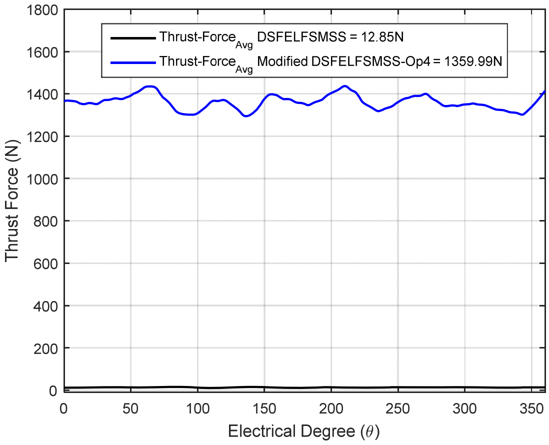

Figure 17. Thrust force comparison

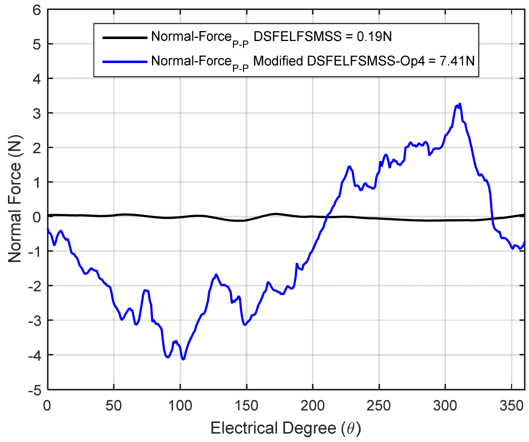

Figure 18. Normal force comparison

TABLE XII. QUANTITATIVE COMPARISON OF DSFELFSMSS AND MODIFIED DSFELFSMSS-OP4

Key Performance Indicator (Unit)	**Proposed Machine's Performance**	
	DSFELFSMSS	**Modified DSFELFSMSS-Op4**
Flux-Linkage$_{p\text{-}p}$ (mWb)	67.20	439.25
Detent-Force$_{p\text{-}p}$ (N)	6.24	184.57
Thrust-Force$_{Avg}$ (N)	12.85	1359.99
Normal-Force$_{p\text{-}p}$ (N)	0.19	7.41
TFRR (%)	41.22	9.46

V. CONCLUSION

Proposed double sided Field Excited Linear Flux Switching Machines (FELFSMs) have reduced manufacturing cost due to: (a) segmented secondary; that reduces stator iron volume, and (b) DC field coil excitation, when compared with Permanent Magnet Linear Flux Switching Machines having continuous long secondary. First contribution of this paper is to quantitatively compare dual stator and dual mover topology having same design dimensions with a valid selection of dual stator FELFSM with Segmented Secondary. Geometry based deterministic optimization approach to optimize nine geometry parameters followed by search for appropriate AC and DC current densities without any special cooling arrangements is second contribution. Finally, novel thrust force ripple ratio reduction technique termed as auxiliary end tooth DC winding is successfully examined and introduced. All aforementioned efforts resulted in decrease of thrust force ripple ratio from 41.22% to 9.46% and an increment of 105 times is observed in average thrust force value.

REFERENCES

[1] R. Cao, M. Cheng, C. C. Mi, W. Hua, "Influence of leading design parameters on the force performance of a complementary and modular linear flux-switching permanent-magnet motor," IEEE Trans. Ind. Electron. , vol. 61, no. 05, pp. 2165-2175, May 2014. doi: 10.1109/TIE.2013.2271603.

[2] B. Zhang, M. Cheng, M. Zhang, W. Wang, Y. Jiang, "Comparison of modular linear flux-switching permanent magnet motors with different mover and stator pole pitch," in Proc. 20th International Conference on Electrical Machines and Systems, Australia, 2017, pp. 1–5. doi: 10.1109/ICEMS.2017.8056000

[3] N. Ullah, M. K. Khan, F. Khan, A. Basit, W. Ullah, T. Ahmad, N. Ahmad, "Comparison of Analytical Methodologies for Analysis of Single Sided Linear Permanent Magnet Flux Switching Machine: No-Load Operation," ACES Journal, vol. 33, no. 8, pp. 923-930, Aug. 2018.

[4] A. Gandhi, A. Mohammadpour, S. Sadeghi, L. Parsa, "Doubled-sided FRLSM for long-stroke safety-critical applications," in Proc. 37th Annual conference of the IEEE Industrial Electronics Society, Australia, 2011, pp. 4186-4191. doi: 10.1109/IECON.2011.6119773

[5] Q. Lu, L. Huanwen, H. Xiaoyan, Y. Dingkuan, F. Youtong, Y. Yunyue, "Investigation of double-sided multi-tooth switched-flux linear motor," in Proc. 18th International conference Electrical Machines and Systems, Thailand, 2015, pp. 237-242. doi: 10.1109/ICEMS.2015.7385034

[6] H. Fan, K. T. Chau, C. Liu, L. Cao, T. W. Ching, "Quantitative Comparison of Novel Dual-PM Linear Motors for Ropeless Elevator System," IEEE Trans. Magn., vol. 54, no. 11, Article ID: 8106506, Nov. 2018. doi: 10.1109/TMAG.2018.2842083

[7] N. Ullah, A. Basit, F. Khan, W. Ullah, M. Shahzad, A. Zahid, "Enhancing Capabilities of Double Sided Linear Flux Switching Permanent Magnet Machine," Energies, vol. 11, no. 10, Article ID: 2871, Oct. 2018. doi: 10.3390/en11102781

[8] R. Cao, M. Cheng, W. Hua, X. Wang, W. Zhao, "Modeling of a complementary and modular linear flux-switching permanent magnet motor for urban rail transit applications," IEEE Trans. Energy Conv., vol. 27, no. 02, pp. 489-497, Jun 2012. doi: 10.1109/TEC.2012.2190985

[9] N. Ullah, F. Khan, A. Basit, W. Ullah, M. Shahzad, T. Ahmad, U. Khalid, "Performance comparison and optimization of dual mover linear permanent magnet flux switching machine," IET-Electric Power Applications, March. 2019. doi:10.1049/iet-epa.2018.5820

[10] W. Zhao, M. Cheng, J. Ji, R. Cao, Y. Du, F. Li, "Design and analysis of a new fault-tolerant linear permanent-magnet motor for maglev transportation applications," IEEE Trans. Appl. Supercond., vol. 22, no. 03, pp. 1-4, Jun 2012. doi: 10.1109/TASC.2012.2185209

[11] Y. Du, N, Jin, "Research on characteristics of single-sided linear induction motors for urban transit," in Proc. International conference Electrical Machines and Systems, Japan, 2009, pp. 1-4. doi: 10.1109/ICEMS.2009.5382925

[12] L. Huang, H. Yu, M. Hu, H. Liu, "Study on a long primary flux-switching permanent magnet linear motor for electromagnetic launch systems," IEEE Trans. Plasma Sci., vol. 41, no. 05, pp. 1138-1144, May 2013. doi: 10.1109/TPS.2013.2251478

[13] J. A. Duan, H. B. Zhou, N. P. Guo, "Electromagnetic design of a novel linear maglev transportation platform with finite-element analysis," IEEE Trans. Magn., vol. 41, no. 01, pp. 260-263, Jan. 2011. doi: 10.1109/TMAG.2010.2087388

[14] N. Hodgins, O. Keysan, A. S. McDonald, M. A. Mueller "Design and testing of a linear generator for wave energy applications," IEEE Trans. Ind. Electron., vol. 59, no. 05, pp. 2094-2103, May 2012. doi: 10.1109/TIE.2011.2141103

[15] J. Liu, L. Huang, H. Yu, C. Wen, W. Zhong, "Study on the characteristics of a novel six-phase fault-torrent linear permanent magnet machine for linear oil pumping," IEEE Trans Appl. Supercond., vol. 24, no. 03, Article ID: 5000305, June 2014. doi: 10.1109/TASC.2013.2295683

[16] J. Ji, S. Yan, W. Zhao, G. Liu, X. Zhu, "Minimization of cogging force in a novel linear permanent-magnet motor for artificial hearts,"

IEEE Trans. Magn., vol. 49, no. 07, pp. 3901-3904, July 2013. doi: 10.1109/TMAG.2013.2247028

[17] A. Gandhi, L. Parsa, "Thrust optimization of a five-phase fault-tolerant flux switching linear synchronous motor," in Proc. 38th Annual conference of the IEEE Industrial Electronics Society, Canada, 2012, pp. 2067-2073. doi: 10.1109/IECON.2012.6388740

[18] F. Xiao, Y. Du, Y. Sun, H. Zhu, W. Zhao, W. Li, T. W. Ching, C. Qiu, "A novel double-sided flux-switching permanent magnet linear motor," J. Appl. Phys., vol. 117, no. 17, Article ID: 17B530, Feb. 2015. doi: 10.1063/1.4919271

[19] C. T. Liu, C. C. Hwang, P. L. Li, S. S. Hung, P. Wendling, "Design Optimization of a Double-Sided Hybrid Excited Linear Flux Switching PM Motor With Low Force Ripple," IEEE Trans. Magn., vol. 50, no. 11, Article ID: 8102704, Nov. 2014. doi: 10.1109/TMAG.2014.2322630

[20] R. Cao, Y. Jin, Y. Zhang, M. Cheng, "Design and comparison of two kinds of primary wound field flux-switching linear motors," COMPEL-The international journal for computation and mathematics in electrical and electronic engineering, vol. 37, no. 01, pp. 333-356, Jan. 2018. doi: 10.1108/COMPEL-09-2016-0406

[21] A. Gandhi, L. Parsa, "Thrust optimization of flux-switching linear synchronous machine with yokeless translator," IEEE Trans. Magn., vol. 49, no. 04, pp. 1436-1443, April 2013. doi: 10.1109/TMAG.2012.2221275

[22] N. Ullah, A. Basit, F. Khan, Y. A. Shah, A. Khan, O. Waheed, A. Usman, "Design and Optimization of Complementary Field Excited Linear Flux Switching Machine With Unequal Primary Tooth Width and Segmented Secondary," IEEE-Access, Vol. 7, 2019. doi: 10.1109/ACCESS.2019.2932791

[23] M. F. Omar, E. Sulaiman, M. Jenal, R. Kumar, and R. N. Firdaus, "Magnetic flux analysis of a new field-excitation flux switching motor using segmental rotor," IEEE Transactions on Magnetics, vol. 53, no. 11, pp. 1–4, Nov 2017. doi: 10.1109/TMAG.2017.2703831

[24] J. Zhao, Q. Mou, K. Guo, X. Liu, J. Li, and Y. Guo, "Reduction of the Detent Force in a Flux-Switching Permanent Magnet Linear Motor," IEEE Transactions on Energy Conversion, vol. 34, no. 3, pp. 1695-1705, Sept. 2019. doi: 10.1109/TEC.2019.2916304

[25] Q. Lu, H. Li, X. Huang, and Y. Ye, "Research on yokeless double-sided multi-tooth flux-switching linear motor," COMPEL-The international journal for computation and mathematics in electrical and electronic engineering, vol. 35, no. 02, pp. 832-843, 2016. doi: 10.1108/COMPEL-12-2015-0438